

# Applications of Automated Grey-Field Polariscopes

Jon R. Lesniak<sup>1</sup>, Michael J. Zickel,<sup>1</sup>

## Introduction

Reflective photoelastic strain analysis secured its place in history as one of the earliest forms of full-field stress/strain analysis[1]. It has proven to be very effective over the years, but, because of the technique's maturity, it is often overlooked by younger scientists as fertile ground for innovation. The fundamental principals of photoelasticity were reviewed and mated with modern video and computer technologies to create the grey-field polariscopes[2]. Although photoelasticity needs to keep pace with the turn key era, it is also important that advances in the technology do not inhibit other recent improvements to the technology[3,4]. Furthermore, a simple and easily understandable description of the mechanics of the polariscopes is essential. One must feel comfortable with the measurement being made without requiring extensive study. By combining a rotating analyzer and a video lock-in system an automated grey-field polariscopes has been devised that painlessly collects both magnitude and direction data without user intervention. Although the new polariscopes is capable of making multiple fringe measurements, it has its greatest impact in sub-fringe applications where the output parallels the description of the strain state of an object given by Mohr's circle.

## Grey-field Polariscopes

Figure 1 is a simplified portrayal of the grey-field polariscopes. The object is illuminated with circularly polarized light. Upon propagation through a birefringent medium, or strained photoelastic coating, the light exits elliptically polarized. The components of the light vector on the major and minor axes can be described as

$$A_{maj} = a \cos \left( \frac{\pi}{4} - \frac{\pi}{2} \right) \cos \left( t + \frac{\pi}{4} \right) \quad (1a)$$

$$A_{min} = a \cos \left( \frac{\pi}{4} + \frac{\pi}{2} \right) \sin \left( t + \frac{\pi}{4} \right) \quad (1b)$$

where

$$= f \left( \frac{\pi}{4} - \frac{\pi}{2} \right) \quad (2)$$

where f is the fringe value of the coating [5]

The major axis of the ellipse is always shifted  $\pi/4$  radians from the direction of the first principal strain for odd fringes and  $-\pi/4$  for even fringes (Fig. 2).

If an analyzer is placed in the system at an orientation  $\theta$  from the major axis the resulting light amplitude is described by

$$A = \cos \theta A_{maj} + \sin \theta A_{min} \quad (3)$$

The intensity of the resulting light is related to the square of the amplitude which after several trigonometric manipulations yields

$$I = A^2 = \frac{a^2}{2} [1 + \cos(2\theta) \sin \phi] \quad (4)$$

If the analyzer is allowed to rotate at an angular frequency  $\omega$  then

$$\theta = \omega t - \frac{\pi}{4} \quad (5)$$

It is assumed that the analyzer is parallel with the reference orientation at  $t=0$ . In terms of time, the intensity map is described by

$$I = \frac{a^2}{2} [1 + \sin 2(\omega t - \frac{\pi}{4}) \sin \phi] \quad (6)$$

From this relation it can be seen that in the absence of birefringence ( $\phi = 0$ ) the output is a neutral grey. It can also be seen that in the presence of birefringence the amplitude of the signal oscillates about this neutral grey level. The oscillating portion of the signal is zero when the axis of the analyzer coincides with the principal strain axes. It should also be noted that only the amplitude measurement is affected by the color of the input light. The orientation of the major axis is unaffected.

Sub-fringe PSA assumes small retardation angles so that the amplitude of the oscillations can be directly related to the amplitude of the shear strains. For very small retardation angles Eq. 6 can be rewritten as

$$I = \frac{a^2}{2} [1 + \sin 2(\omega t - \frac{\pi}{4}) \sin \phi] \quad (7)$$

For larger angles some linearization may be required.

## Video Lock-in

In order to make extremely accurate measurements of sub-fringe birefringence, a video lock-in algorithm is employed. The analyzer and an absolute position encoder are rotated at a constant angular velocity while the computer monitors the output of the encoder. When a prescribed angle is crossed an image is captured and stored for subsequent processing. In this study eight images are captured for every one half revolution of

<sup>1</sup> Stress Photonics Inc., 3002 Progress Rd., Madison, WI 53716

the analyzer. The angles at which the computer triggers the capture of an image are defined by

$$\theta_n = \frac{(n-1)\pi}{N} \quad (8)$$

It is important to recall that a full period of signal oscillation is represented by one half of an analyzer revolution.

By controlling the image sampling in this manner a level of synchronization is achieved and the lock-in algorithm that is performed takes the simple form described by

$$I_n(x,y) = \frac{2}{N} \sum_{n=1}^N J_n(x,y) \sin(2\theta_n) \quad (9a)$$

$$I_n(x,y) = \frac{2}{N} \sum_{n=1}^N J_n(x,y) \cos(2\theta_n) \quad (9b)$$

where  $J_n$  is a sampled image. From Eqs. 9(a,b) the amplitude and direction of shear strains can be determined by the following relations

$$K = \sqrt{\epsilon_x^2 + \epsilon_y^2} \quad (10)$$

where K is a calibration constant including system gains, light intensity variations and residual strains in the coating. The phase is calculated from the X and Y images as

$$\theta = \tan^{-1} \left( \frac{Y}{X} \right) \quad (11)$$

The orientation of the first principal strain direction to the reference direction ( $\theta_1$ ) is related to  $\theta$  by

$$\theta_1 = \frac{\theta}{2} \quad (12)$$

For odd fringes  $\theta_1$  points in the direction of the first principal strain, and for even fringes  $\theta_1$  points in the direction of the second principal strain.

The results of Eqs. 10–12 are identical to the equations describing Mohr's circle for plane strain where X is the base, Y is the height and the angle  $\theta_1$  represents the physical angle on the specimen. This means that the results of this polariscope directly yield in-plane shear strain components for any arbitrary direction. Also, this implies that in the linearized area, the XY image sets can be operated on as vectors. The superposition of two strain states can be calculated by adding two XY image pairs then applying Eqs. 10-12 to find magnitude and direction. To remove the effects of residual strain in the coating an initial XY pair can be captured and subtracted from the images collected during loading. The magnitude and direction are then calculated after the subtraction.

### Experimental Setup

A simple yet flexible optical setup was used. The light source consists of a standard light bulb which projects white light through a condenser lens, a filter (optional), a polarizer and, finally, a quarter waveplate. Circularly polarized light is projected onto the area of interest.

The camera system is comprised of a zoom lens, rotating analyzer, and video detector. Currently filters are used to narrow the pass bands of the incoming light to 40 nm width. The rotating analyzer is positioned near the detector. The angular position of the analyzer is monitored by the absolute position encoder. The computer monitors the status of this encoder and triggers the frame-grabber at predetermined angles. As mentioned above the use of predetermined angles allows the use of a simple lock-in algorithm. The sampled images are processed by the computer and displayed in both magnitude and direction.

### Coating

A special tinted coating is employed to facilitate automatic thickness measurement. The tint transmits the red light, partially attenuates the green and absorbs the blue light (Fig. 3). A simple relation for thickness is obtained as

$$Thickness = \ln \frac{G - B}{R - B} \quad (13)$$

where the blue light is used to subtract out the level of reflected light and the red light is used to normalize for intensity. Figure 4 shows the thickness map for a coating thickness gradient of 0.15 mm to 1.0 mm.

### Light Intensity and System Gain

Light intensity variations and pixel by pixel system gains can be determined separately or together. The following is a simple approach to calibrate the above mentioned parameters and to establish the correct phase of the lock-in, which effectively sets the reference orientation. To accomplish all of the above in the sub-fringe mode a calibration plate of birefringence can be introduced into the system just before the analyzer to augment the existing birefringence. This apparent strain can be resolved by subtraction of the loaded image from the loaded-augmented image. From this information light intensity can be calculated free of reflection error.

An alternative to this approach is to use the average of the X and Y (Eqs. 9a and 9b) images as the intensity and to calibrate the system gains separately. This approach will be more important as the speed of grey-field polariscope systems increases and dynamic strains are monitored.

### Residual Strains

Residual strains can be eliminated simply by load differencing. Essentially an image is run through the paces as described above, and then the load is increased and the process is repeated. The difference between these images will compensate for residual strains and/or light source imperfections.

### Load Ramping

Load ramping is also useful for imaging large or complex components that exhibit a wide range of strain values. With this technique a low load is initially used so that regions exhibiting

high strain fields can be interrogated with good resolution and without exceeding sub-fringe limitations. The load is then increased so that regions with lower strain values can be sampled with optimal resolution. By using the load ramping technique all regions on the sample can be inspected with optimal resolution. The extent of the dynamic range of the response defines the number of loads that should be used. This method can significantly increase the apparent dynamic range.

## Results

A beam in four-point bending was used as the test specimen. The beam (3.175 mm thick aluminum) was coated with a commercially available photoelastic sheet coating (0.254 mm thick) and loaded at approximately 1kN. In this example it can be seen that the grey-field polariscope can distinguish between shear strains created by a tensile stress at the top of the beam and a compressive stress at the bottom of the beam (Fig 5). The indicators align themselves with the direction of the first principal strain, which for compression is orthogonal to the direction of applied stress. The Shear 0 degree image is null because there are no shear strains in the horizontal/vertical orientation. The shear strains are maximum along the 45 degree planes, so all strain information is contained in the shear 45 degree image.

## Conclusion

A fully automated polariscope system that determines the magnitude and direction of the shear strains has been developed. This grey-field polariscope also automatically distinguishes between the directions of the principal strains, and indicates each direction in the resultant data. The data are presented in an intuitive format so that they are easy to interpret. One image depicts the shear strain magnitude with gradients represented in greyscale levels, and the other indicates the directions of the principal strains. Interpretation of the data parallels the strain state description given by Mohr's circle for plane strain.

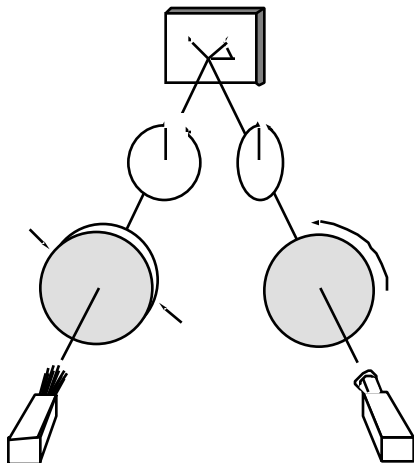


Figure 1. Grey-field reflection polariscope

The grey-field polariscope utilizes a video lock-in algorithm to achieve a high degree of sensitivity, which makes it ideal for subfringe operation. This does not exclude higher order fringe operation, where techniques such as load ramping can be used to great advantage.

## Acknowledgments

The authors would like to acknowledge NASA Langley Research Center and in particular Mr. K. Elliott Cramer for supporting this research through the STTR (Small Business Technology Transfer) program. In addition, Mr. Dan Bazile and Jim Krzoska of Stress Photonics Inc. contributed extensively in the design and construction of the polariscope and light source.

## References

- [1] Zandman, F., "Photostress Analysis," Product Engineering, March, 43-46, 1959.
- [2] Lesniak, J. R., Zickel, M. J., Welch, C. S., Johnson, D. F., "An Innovative Polariscope for Photoelastic Stress Analysis," to be published in Proc. Soc. for Exp. Mech., Spring Conf., June 1997.
- [3] Barone, S., Patterson, E. A., "Full-field Separation of Principal Stresses by Combined Thermo- and Photoelasticity," Experimental Mechanics, Vol. 36, No. 4, December, 318-324, 1996.
- [4] Asundi, A., "Phase Shifting in Photoelasticity," Experimental Techniques, January/February, 19-23, 1993.
- [5] Measurements Group Tech Note, TN-701, Measurements Group, Inc., P.O. Box 27777, Raleigh, NC, 1977.

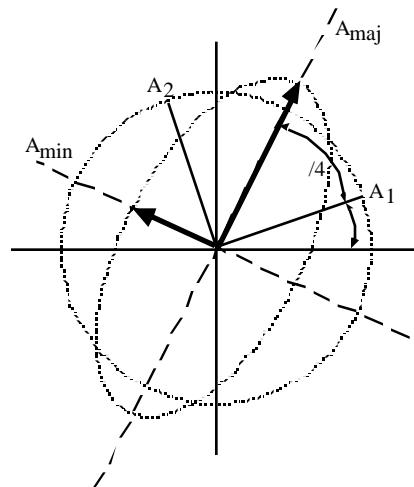


Figure 2. Elliptically polarized light

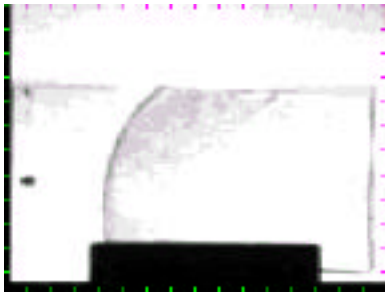
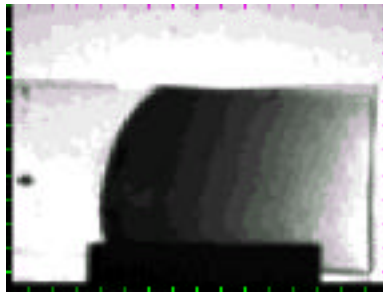


Fig. 3 Red image

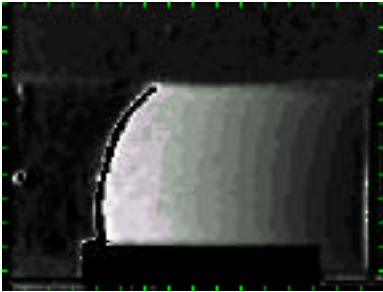


b) Green image

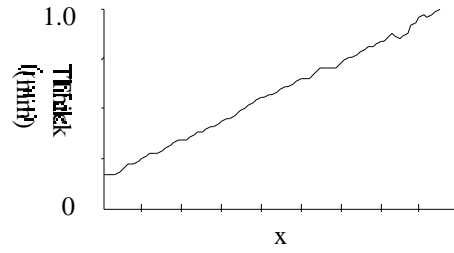


c) Blue image

Fig. 3 RGB transmittance through tinted coating

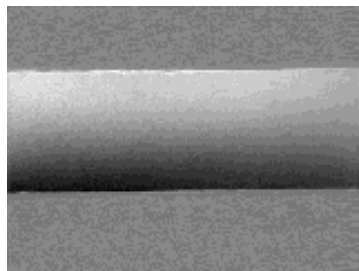


a) Thickness map



b) Thickness profile

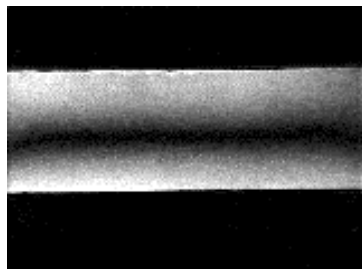
Fig. 4 Thickness measurements



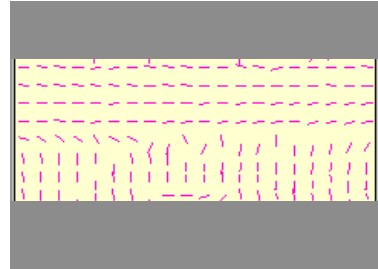
a) X image (Shear 45 degree)



b) Y image (Shear 0 degree)



c) Magnitude



d) Direction

Fig. 5 Images showing the magnitude and the direction of principal strains